Fast-Processing Sigma-Delta Strategies for Three-Phase Wide-Bandgap Power Converters with Common-Mode Voltage Reduction

David Lumbreras, *Graduate Student Member, IEEE,* Jordi Zaragoza, *Member, IEEE,* Néstor Berbel, Juan Mon, Eduardo Gálvez and Alfonso Collado

***Abstract*—The electromagnetic compatibility of wide-bandgap (WBG) power converters can be greatly improved using spread-spectrum modulation techniques. This article proposes a family of reduced common-voltage sigma-delta modulations (RCMV-ΣΔ) for voltage source converters (VSC) that use gallium nitride (GaN) semiconductors. Specifically, this article proposes three new techniques: two reduced-state sigma-delta modulations (RS-ΣΔ1&2) and an active sigma-delta strategy (A-ΣΔ). The proposed modulation techniques reduce or eliminate the common-mode voltage (CMV) dv/dt transitions and suppress the noise spikes in the conducted electromagnetic interference (EMI) spectrum. Furthermore, this article proposes the use of fast-processing quantizers for RCMV-ΣΔ techniques as well as for hexagonal sigma-delta (H-ΣΔ). These quantizers use a novel calculation methodology that simplifies the implementation of the proposed modulations and considerably reduces their computational cost. The performance and the total harmonic distortion of RCMV-ΣΔ techniques are analysed here using MATLAB/Simulink and PLECS. Experimental results performed on a VSC converter that uses GaN e-HEMTs show how RCMV-ΣΔ techniques considerably improve electromagnetic compatibility and exhibit similar efficiencies and total harmonic distortions (THD) to those of H-ΣΔ.**

***Index Terms*—Common-mode voltage, electromagnetic compatibility (EMC), fast algorithm, modulation techniques, power electronics, sigma-delta (ΣΔ) modulation, vector quantization, voltage source converter (VSC), wide-bandgap (WBG) semiconductors**

I. Introduction

WIDE-BANDGAP (WBG) power converters exhibit superior properties to conventional silicon-based converters. These new power converters show excellent efficiency and may have a high power density. Moreover, they can work at extremely high switching frequencies with fewer losses than their silicon counterparts [1], [2]. The two most mature WBG semiconductors are gallium nitride (GaN) and silicon carbide (SiC). In general, GaN has better properties than SiC, but GaN devices are limited to low-voltage applications (<650 V), whereas SiC devices are preferred for high-voltage operations [2]. GaN devices have already been successfully used in numerous power electronics applications, such as microgrids [3], [4], wireless chargers [5], electric vehicle (EV) battery chargers [6], on-board chargers [7], ac electric drives [8], [9], electric vehicles [10], and resonant converters [11].

David Lumbreras is with the Terrassa Industrial Electronics Group, Department of Electronic Engineering, Universitat Politècnica de Catalunya (UPC), 08222 Terrassa, Spain, and also with the R&D Power Electronics, Circutor S.A., 08232 Viladecavalls, Spain (e-mail: david.lumbreras@upc.edu).

Jordi Zaragoza, Néstor Berbel, and Juan Mon are with the Terrassa Industrial Electronics Group, Department of Electronic Engineering, Universitat Politècnica de Catalunya (UPC), 08222 Terrassa, Spain (e-mail: jordi.zaragoza-bertomeu@upc.edu; nestor.berbel-artal@upc.edu; juan.mon@upc.edu).

Eduardo Gálvez and Alfonso Collado are with the R&D Power Electronics, Circutor S.A., 08232 Viladecavalls, Spain (e-mail: egalvez@circutor.com; acollado@circutor.com).

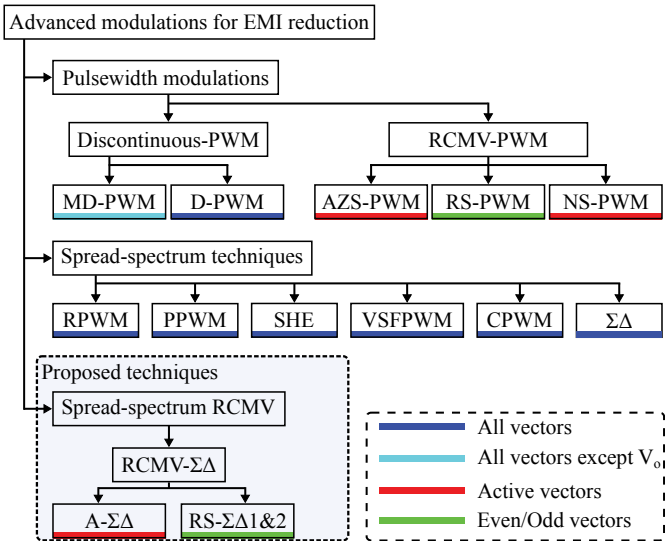

Fig. 1. Modulation strategies for EMI reduction in three-phase two-level voltage source converters.

The low switching losses of WBG semiconductors are due to their high switching speed, i.e., high dv/dt voltage slew rates. This fast switching speed, combined with a high switching frequency, increases common-mode electromagnetic interference (EMI) [12], [13]. High common-mode voltages (CMV) can cause several problems. In electric motors, CMV can cause bearing currents, electromagnetic interferences, induced shaft voltages, mechanical vibrations, and winding insulation damage [14]–[16]. In photovoltaic systems, common-mode voltages often generate common mode currents (CMC). These currents may increase the power losses and distort the output voltages and currents [17], [18].

A common and effective method to reduce EMI is to use advanced modulation techniques (see Fig. 1). There are two main modulation families to reduce EMIs. First, there is the group of pulsewidth modulation (PWM) techniques [14]. These

modulations compare a modulating signal to fixed frequency triangular signals, so the switching frequency is constant. A zero-sequence is added to the modulating signal to modify its shape and, thus, the behaviour of the modulation. Within this family of techniques, there are the discontinuous (D-PWM) and the reduced common-mode voltage pulsewidth modulations (RCMV-PWM). D-PWM strategies reduce switching losses by decreasing transitions in a switching period [14], [19]. Consequently, the switching losses and the common-mode voltage are reduced. RCMV-PWM techniques improve electromagnetic compatibility because they avoid applying zero vectors, i.e., those that generate the highest levels of CMV [14], [19]–[21]. Recent works study the benefit of PWM techniques and even propose new modulations. Reference [22] analysed the influence of the active zero-state pulsewidth modulation (AZS-PWM) on the design of the EMI filters. In [16], the AZS-PWM technique was implemented in a SiC-based converter. This article demonstrated that the modulation limits the shaft voltage in ac electric drives. Finally, a new generalized tri-state pulsewidth modulation for high-frequency voltage source converters (VSC) was introduced in [23]. Compared to other RCMV-PWM, this technique may reduce the switching losses and improve the harmonic distortion. Secondly, there are the spread-spectrum techniques. These modulations vary the switching frequency. Hence, they improve the converter efficiency, lower the switching harmonics, and spread them over a broad frequency range [24]. Many articles investigate the qualities of these modulations. The effect of random modulation (RPWM) on EMI emission in VSCs was widely investigated in [25]. In [26], the authors designed and optimised periodic modulations (PPWM) for active power filters. Finally, a new family of PPWM techniques based on the distribution characteristics of switching frequency was proposed in [27]. Although all of these techniques may reduce EMI, they usually exhibit lower efficiency or higher total harmonic distortion (THD) than the classical space vector pulsewidth modulation (SVPWM) [14].

An interesting spread-spectrum modulation technique is sigma-delta modulation ($\Sigma\Delta$), which first appeared in the early 1960s [28], [29]. Nowadays, it is used in audio applications, digital power amplifiers, digital-to-analog converters, and sample-rate converters [30]. $\Sigma\Delta$ modulation is also relevant for power converters since their high switching frequencies guarantee a good resolution [31]. Initially, $\Sigma\Delta$ was applied to resonant converters [32], [33]. Later, Luckliff *et al.* proposed using a hexagonal quantizer to improve the modulation. This new strategy was patented and called hexagonal sigma-delta modulation (H-$\Sigma\Delta$) [31], [34], [35]. Recently, the usefulness of this technique was demonstrated for high-frequency WBG power converters [36], including for five-phase VSCs [37]. H-$\Sigma\Delta$ exhibits an excellent efficiency and very low total harmonic distortion for switching frequencies from 100 kHz upwards. Nevertheless, the H-$\Sigma\Delta$ technique needs complex calculations to determine the switching state. Some authors have proposed simplified quantizers for other $\Sigma\Delta$ modulations, but these quantifiers still require complex transformations and multiple mathematical operations [38].

None of the previous articles proposes modulations that combine the properties of RCMV-PWM and spread-spectrum techniques, although in [39], the authors study a combined $\Sigma\Delta$ modulation capable of suppressing the CMV in matrix converters.

This article studies and proposes a family of RCMV-$\Sigma\Delta$ modulations that combine the benefits of H-$\Sigma\Delta$ modulation with those of RCMV-PWM techniques. Three RCMV-$\Sigma\Delta$ strategies are proposed: two reduced-state sigma-delta modulations (RS-$\Sigma\Delta$1&2) and an active sigma-delta strategy (A-$\Sigma\Delta$). These modulations are suitable for high-frequency three-phase VSC converters based on WBG semiconductors. The proposed modulations allow the following:

1) reducing common-mode voltages and currents and, consequently, reducing the EMIs;
2) maintaining the same THD level and performance as H-$\Sigma\Delta$ modulation, thus overcoming the classical SVPWM [36] without the problems exhibited by other RCMV-PWM modulations [14].

Moreover, we propose fast-processing quantizers for RCMV-$\Sigma\Delta$ techniques but also for the classic H-$\Sigma\Delta$. These quantizers greatly simplify the implementation of the proposed modulations and require fewer mathematical operations than a standard quantizer. The impact of RCMV-$\Sigma\Delta$ strategies is evaluated on the basis of simulation studies using the software MATLAB/Simulink and PLECS. Finally, the results are experimentally validated by implementing the proposed techniques on a GaN-based VSC converter.

The rest of this article is organized as follows. Section II summarizes $\Sigma\Delta$ modulation and analyses its basis. Section III introduces RCMV-$\Sigma\Delta$ techniques and presents the novel fast-processing quantizers. Section IV analyses the behaviour of the proposed techniques. Section V validates the above results that showed the impact of the modulation techniques on real power converters. Finally, Section VI summarizes the conclusion of this article.

II. Basis of the Sigma-Delta

The proposed RCMV-$\Sigma\Delta$ strategies share the modulation loop structure with the H-$\Sigma\Delta$ technique (see Fig. 2) [36]. The single-loop RCMV-$\Sigma\Delta$ modulations are drawn using solid black lines, while the dashed red lines mark the additional elements present in the double-loop strategies.

To analyse the proposed modulation, it is necessary to define the plane $Q = \{(\alpha, \beta, \gamma) \in \mathbb{R}^3 \mid \gamma = 0\}$. $W : \mathbb{R}^3 \to Q$ is then defined as

$$W = \frac{2}{3}\begin{bmatrix} 1 & -\frac{1}{2} & -\frac{1}{2} \\ 0 & \frac{\sqrt{3}}{2} & -\frac{\sqrt{3}}{2} \\ 0 & 0 & 0 \end{bmatrix} \tag{1}$$

which is a simplified Clarke transformation.

The proposed techniques work in $\alpha\beta\gamma$ frame, so it is necessary to express the reference vector (V_{ref}) in these coordinates using W. Once $V_{ref} \in Q$, the modulation compares it (V_α, V_β) to the outputs of the quantizer (V'_α, V'_β) and integrate the resulting errors (e_α, e_β). Before each integration, there are gains whose value may be adjusted. The value of these gains

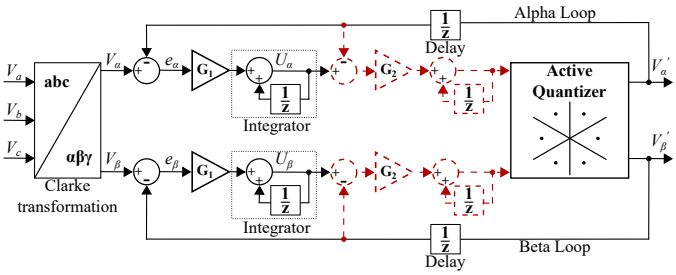

Fig. 2. Reduced common-mode voltage sigma-delta loop. The second integrator loop is drawn with dashed red lines. The nominal value of all gains is unity.

affects the output noise and system stability [40]. In [36], a stability analysis of ΣΔ techniques is performed.

The integrated errors (U_α, U_β) are the inputs of the quantizer, whose outputs are compared to the next reference vector. Before the quantizer, more integrators can be included in the loop to improve the modulation (see Fig. 2). A maximum of two integrators should be used since the modulation becomes noisy when three or more integrators are introduced [40]. The equation that describes an N-loop ΣΔ is

$$V'_x(z) = V_x(z)z^{-1} + e_x(z)(1 - z^{-1})^N \tag{2}$$

where $x = \{\alpha, \beta\}$, and N is the number of integrators.

The quantizer divides the Q-plane into various sectors, which are the Voronoi cells of the power converter's switching vectors. At every sampling instant, the quantizer determines the position of the input (i.e., the integrated error) and synthesizes it by applying the nearest switching vector. The closest switching vector is found with

$$D_i^2 = (V'_{\alpha i} - U_\alpha)^2 + (V'_{\beta i} - U_\beta)^2 \tag{3}$$

where D_i^2 is the Euclidean distance squared from the integrated error (U_α, U_β) to the switching state $(V'_{\alpha i}, V'_{\beta i})$.

The point that is closest to the reference is the switching vector with the minimum value of D_i^2. Furthermore, using branch and bound algorithms (B&B) may reduce the number of calculations [36]. However, the implementation of the quantizer can be improved using a different approach. This is further studied in Section III-A. Once the nearest vector is found, the switching state of the inverter is determined.

III. Proposed Sigma-Delta strategies

The objective of RCMV-ΣΔ techniques is to reduce common-mode voltage and conducted EMIs. Therefore, these techniques use active quantizers. These quantizers work with the projections in Q of the active vectors. Consequently, the converter never applies zero vectors, and the CMV is minimized.

Active quantizers differ depending on the ΣΔ technique. The proposed RS-ΣΔ1 modulation uses only the odd vectors (V_1, V_3, V_5), while the RS-ΣΔ2 strategy solely employs the even vectors (V_2, V_4, V_6). Therefore, these techniques only apply vectors that generate the same level of CMV, so they suppress the dv/dt transitions. The quantizers of both RS-ΣΔ1&2 techniques divide the Q-plane into three sectors,

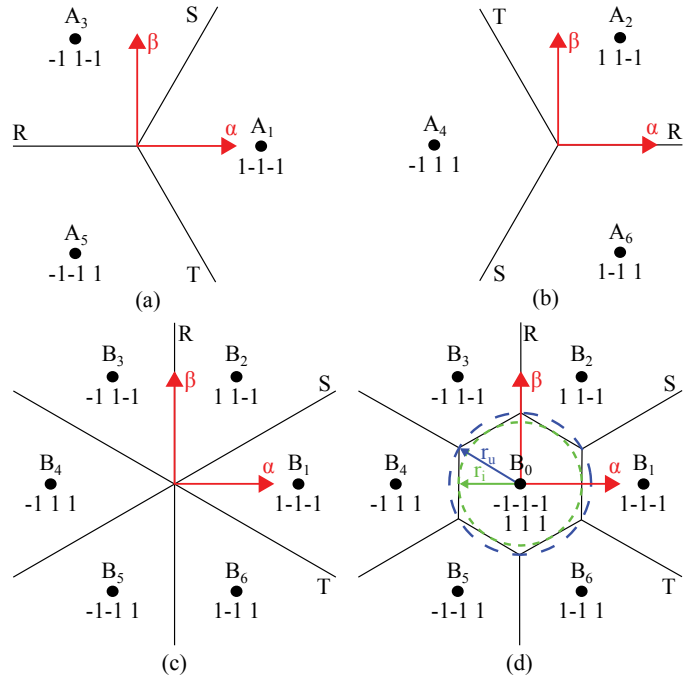

Fig. 3. Two-level vector diagram divided into sectors according to (a) RS-ΣΔ1, (b) RS-ΣΔ2, (c) A-ΣΔ, and (d) H-ΣΔ.

one for each possible vector. Nevertheless, using only three active vectors greatly reduces the linear range of the RS-ΣΔ1&2 techniques, since $|V_{ref}|_{max} = 0.33V_{dc}$ and, thus, $m_a = 0.57\frac{2}{\sqrt{3}}$. The third proposed modulation, the A-ΣΔ, uses all of the active vectors, so its linear range is not reduced. Hence, this technique does not eliminate the dv/dt transitions but reduces their height. Its quantizer divides Q into six sectors, which are the Voronoi cells of a VSC's active vectors. Fig. 3 depicts the division of the Q-plane according to the proposed quantizers. The switching states are represented by -1 and 1, which indicate, respectively, the output voltage levels of $\frac{-V_{dc}}{2}$ and $\frac{V_{dc}}{2}$ that correspond to the midpoint of the dc bus.

Table I summarizes the features of the proposed techniques and compares them with the classical SVPWM modulation.

A. Proposed quantization method

This section proposes a novel implementation of a quantifier for the proposed RCMV-ΣΔ techniques and also for the well-known H-ΣΔ modulation. The proposed method simplifies the implementation of the quantizer and also reduces the number of calculations required.

The Q-plane is divided into Voronoi regions. The boundaries of these sectors are determined by the straight lines R, S, and T (see Fig. 3). These lines are defined as follows:
Lines for RS-ΣΔ1&2:

$$R = \{(\alpha, \beta) \mid \beta = 0\}, \tag{4}$$

$$S = \{(\alpha, \beta) \mid \frac{\alpha}{k} - \beta = 0\}, \tag{5}$$

$$T = \{(\alpha, \beta) \mid \frac{\alpha}{k} + \beta = 0\} \tag{6}$$

TABLE I
CHARACTERISTICS OF THE MAIN $\Sigma\Delta$ TECHNIQUES COMPARED TO CONVENTIONAL SVPWM

				Proposed RCMV-$\Sigma\Delta$	
		SVPWM[a]	H-$\Sigma\Delta$	A-$\Sigma\Delta$	RS-$\Sigma\Delta$1&2
Linear range		$0 \leq m_a \leq 1.15$	$0 \leq m_a \leq 1.15$	$0 \leq m_a \leq 1.15$	$0 \leq m_a \leq 0.66$
Voltage vectors used		All vectors	All vectors	Active vectors	Even/Odd vectors
Maximum switching frequency (f_{max})		$1/{T_s}^b$	$1/2{T_s}^b$	$1/2{T_s}^b$	$1/2{T_s}^b$
CMV-related data	CMV waveform during three ${T_s}^b$	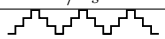	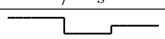	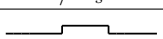	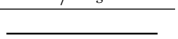
	Peak-to-peak value relative to V_{dc}	1	1	1/3	0
	Height of largest CMV step relative to V_{dc}	1/3	1	1/3	0
	Number of different levels per ${T_{sw}}^c$	4	1-3	1-2	1
	Number of transitions per ${T_{sw}}^c$	6	0-2	0-2	0

[a] Symmetrical sampled SVPWM [41]. [b] T_s is the sampling period. [c] T_{sw} is the switching period.

where $k = \tan(\pi/6)$.
Lines for H-$\Sigma\Delta$ and A-$\Sigma\Delta$:

$$R = \{(\alpha, \beta) \mid \alpha = 0\}, \tag{7}$$

$$S = \{(\alpha, \beta) \mid k\alpha - \beta = 0\}, \tag{8}$$

$$T = \{(\alpha, \beta) \mid k\alpha + \beta = 0\}. \tag{9}$$

Using the expressions of the lines, we can define the sectors of Q for the proposed fast modulation techniques as follows:
Sectors for RS-$\Sigma\Delta$1:

$$A_1 = \{x \in Q : (\alpha \geq k\beta) \wedge (\alpha \geq -k\beta)\}, \tag{10}$$

$$A_3 = \{x \in Q : (\beta \geq 0) \wedge (\alpha < k\beta)\}, \tag{11}$$

$$A_5 = \{x \in Q : (\beta < 0) \wedge (\alpha < -k\beta)\}. \tag{12}$$

Sectors for RS-$\Sigma\Delta$2:

$$A_2 = \{x \in Q : (\beta \geq 0) \wedge (\alpha \geq -k\beta)\}, \tag{13}$$

$$A_4 = \{x \in Q : (\alpha < k\beta) \wedge (\alpha < -k\beta)\}, \tag{14}$$

$$A_6 = \{x \in Q : (\beta < 0) \wedge (\alpha \geq k\beta)\}. \tag{15}$$

Sectors for A-$\Sigma\Delta$:

$$B_1 = \{x \in Q : (\alpha \geq 0) \wedge (-k\alpha \leq \beta < k\alpha)\}, \tag{16}$$

$$B_2 = \{x \in Q : (\alpha \geq 0) \wedge (\beta \geq k\alpha)\}, \tag{17}$$

$$B_3 = \{x \in Q : (\alpha < 0) \wedge (\beta \geq -k\alpha)\}, \tag{18}$$

$$B_4 = \{x \in Q : (\alpha < 0) \wedge (k\alpha \leq \beta < -k\alpha)\}, \tag{19}$$

$$B_5 = \{x \in Q : (\alpha < 0) \wedge (k\alpha > \beta)\}, \tag{20}$$

$$B_6 = \{x \in Q : (\alpha \geq 0) \wedge (-k\alpha > \beta)\}. \tag{21}$$

The regions of H-$\Sigma\Delta$ are similar to those of A-$\Sigma\Delta$. However, this technique has an additional hexagonal sector (B_0) corresponding to the Voronoi cell of the zero vectors. When the reference is not within the central hexagon, this technique uses the same equations as the A-$\Sigma\Delta$ modulation to determine the region. The zero sector is assumed to be a circumference to simplify the quantizer. Thus, the sector is defined as follows:

$$B_0 = \{x \in Q : \alpha^2 + \beta^2 \leq r_0^2\} \tag{22}$$

TABLE II
DETERMINATION OF THE SECTOR IN A-$\Sigma\Delta$

$U_\alpha \geq 0$	$U_\beta \geq kU_\alpha$	$U_\beta \geq -kU_\alpha$	Sector	Switching state
0	0	0	B_5	-1-11
0	0	1	—	Do not care
0	1	0	B_4	-111
0	1	1	B_3	11-1
1	0	0	B_6	1-11
1	0	1	B_1	1-1-1
1	1	0	—	Do not care
1	1	1	B_2	11-1

where r_0 is the circumference radius. The circumference with radius r_0 should have a similar size to the original hexagon to minimise the error caused by this approximation. Hence, $r_0 = [r_i, r_u] = [0.67, 0.77]$. This is further studied in Section IV.

Given a point in plane Q, the above expressions allow one to determine to which region it belongs. In RCMV-$\Sigma\Delta$ modulations, the procedure to determine the sector is as follows: First, boundary values of the straight lines R, S, and T are calculated from the input. The boundary points of S and T depend on U_α or U_β, so they have to be calculated for each input. In contrast, the boundary value of R is constant and equal to 0. Once the boundaries are determined, the quantizer compares the input with them. The comparison result is a 3-bit word that is used as the address of read-only memory (ROM). The output of ROM is the nearest vector, as detailed in Tables II and III, for A-$\Sigma\Delta$ and RS-$\Sigma\Delta$1&2, respectively. This output may be the switching state, which allows for the algorithm to be further simplified. ROM also determine the coordinates of the applied vector to close the $\Sigma\Delta$ loop.

The determination of the sector in H-$\Sigma\Delta$ is slightly different. First, it is determined whether the input belongs to B_0 through (22). If the point belongs to that region, the converter applies one of the zero vectors. If not, the quantizer follows the same procedure as in the A-$\Sigma\Delta$ modulation; i.e., the sector is determined as detailed in Table II. Fig. 4 depicts the flowchart of the proposed fast $\Sigma\Delta$ techniques and compares it with the flowchart of a standard H-$\Sigma\Delta$ with branch and bound.

Tables IV and V quantify the operations of the proposed fast quantizers and compare them with those of other quantizers. Standard quantizers determine the nearest vector by

TABLE III
DETERMINATION OF THE SECTOR IN RS-ΣΔ1&2

$U_\beta \geq 0$	$U_\alpha \geq kU_\beta$	$U_\alpha \geq -kU_\beta$	Odd sector (RS-ΣΔ1)	Even sector (RS-ΣΔ2)
0	0	0	A_5	A_4
0	0	1	—	—
0	1	0	A_5	A_6
0	1	1	A_1	A_6
1	0	0	A_3	A_4
1	0	1	A_3	A_2
1	1	0	—	—
1	1	1	A_1	A_2

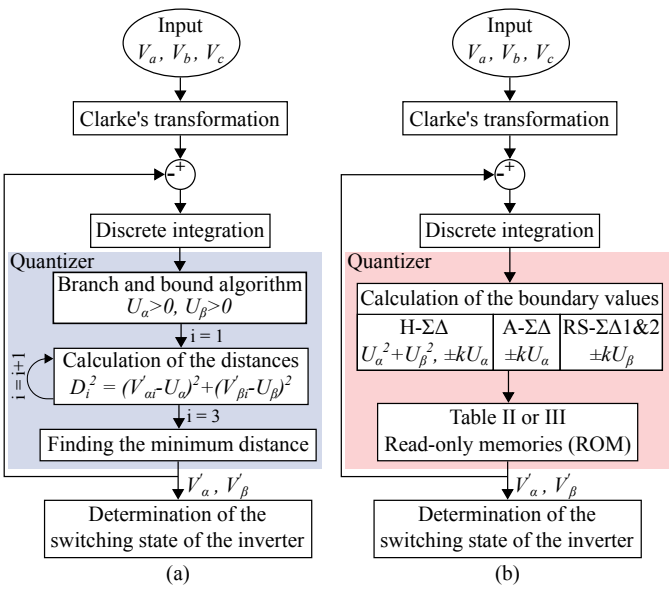

Fig. 4. Flowchart of the ΣΔ techniques. (a) Standard quantizer with branch and bound. (b) Proposed fast quantizers.

calculating distances, i.e., using (3) for each potential vector. Branch and bound algorithms use comparisons to reduce the number of possible vectors. Thus, they limit the mathematical operations performed. However, the proposed quantification methods further reduce the number of calculations performed on the quantizer since the nearest vector is determined without calculating distances. The proposed fast H-ΣΔ requires the same number of comparisons as the B&B algorithm but reduces additions and multiplications, and it does not need subtractions. Furthermore, the presented fast RCMV-ΣΔ techniques require fewer operations than their standard counterparts and also than the fast H-ΣΔ because they do not have a zero sector.

IV. SIMULATION RESULTS

This section evaluates the impact of the proposed RCMV-ΣΔ techniques on the VSC with GaN e-HEMTs. To assess the effects of the proposed modulations, the results are compared with those of the H-ΣΔ.

The switching frequency is variable in ΣΔ modulations. The switching frequency of sigma-delta techniques (f_{sw}) is

$$f_{sw} = \frac{f_s}{n} \tag{23}$$

TABLE IV
OPERATIONS OF THE DIFFERENT QUANTIZERS FOR H-ΣΔ

Operations	Standard quantizer	Standard with (B&B)[a]	Fast H-ΣΔ
Additions	7	3	1
Subtractions	14	6	0
Multiplications	14	6	4
Comparisons	6	4	4
ROM	Yes	Yes	Yes
Total	41	19	9

[a]The branch and bound algorithm is the one presented in [36].

TABLE V
OPERATIONS OF THE DIFFERENT QUANTIZERS FOR RCMV-ΣΔ

Operations	Standard A-ΣΔ	Fast A-ΣΔ	Standard RS-ΣΔ1&2	Fast RS-ΣΔ1&2
Additions	6	0	3	0
Subtractions	12	0	6	0
Multiplications	12	2	6	2
Comparisons	5	3	2	3
ROM	Yes	Yes	Yes	Yes
Total	35	5	17	5

where f_s is the sampling frequency, and n is an integer such that $n \geq 2 \ \forall \ n \in \mathbb{Z} \ (n = 2, 3, 4, ..., \infty)$.

This work uses the maximum switching frequency (f_{max}) as a comparison parameter. In these techniques, the maximum switching frequency is always half the sampling frequency. The modulation index is defined as $m = m_a\sqrt{3}/2$, where m_a is the original modulation index. Thus, m is within the range of [0, 1].

The studied VSC is modelled using MATLAB/Simulink and PLECS Blockset. The rated power of the converter is 5.88 kVA; the dc bus voltage is 400 V; and the ac-side currents are constant at their rated values (15 A). The GaN e-HEMT GS66508T is used to simulate the converter switches. These transistors feature a maximum drain-source voltage (V_{ds}) of 650 V and a continuous drain current (I_d) of 30 A. Each GaN e-HEMT has only an external gate resistance of 10 Ω, the deadtime is 60 ns, and their junction temperatures are 90 ºC. The PLECS software calculates the losses according to the thermal datasheet and the equations provided by the manufacturer [42], [43].

A. Fast algorithm validation

The fast algorithm for H-ΣΔ is validated by implementing the quantizer using three different radii: 0.67 (r_i), 0.72 (r_m), and 0.77 pu (r_u). Fig. 3(d) shows the minimum and maximum radius. Fig. 5 illustrates the errors obtained using the different radii and compares them with those of the conventional H-ΣΔ technique. The average error at different modulation indexes is depicted in Fig. 5(a). The error is measured over 20 ms, i.e., over one electrical grid period. The error is the difference between the reference voltage and the quantizer output. Hence, the error only is zero when one of the eight converter states can fully synthesize the reference voltage. As this happens infrequently, there is always an error. However,

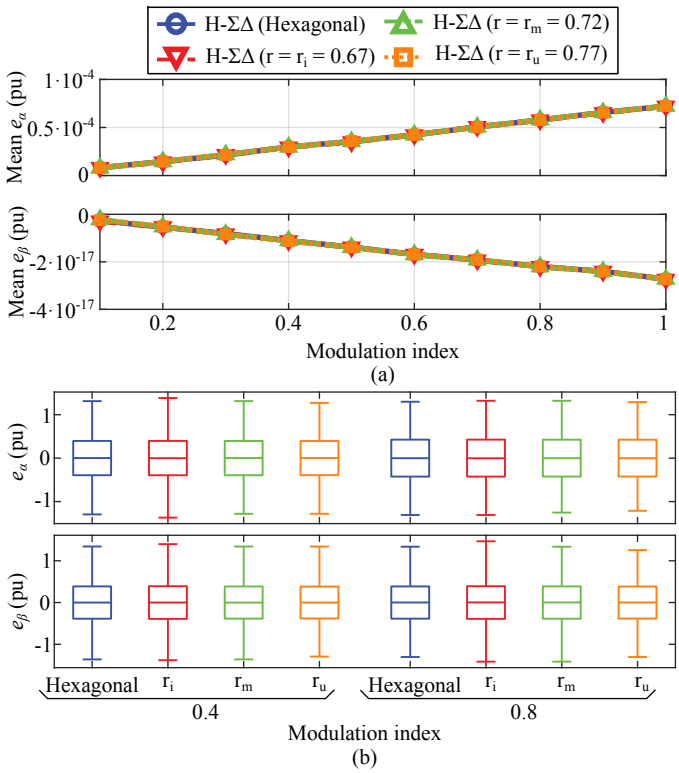

Fig. 5. Influence of the radius r_0 on the H-ΣΔ modulation error. (a) Comparison of the mean error. (b) Error distribution at different modulation indexes.

the modulation minimises this error, so the average error is low, almost zero, for all quantizers. Moreover, there are no appreciable differences between the errors produced by the different quantizers. The mean errors in alpha (e_α) are significantly larger than those in beta (e_β). As in space vector modulations, the reference vector is never equal to vectors 1 and 4. Therefore, in sectors B_1 and B_4, there is an intrinsic error in the alpha axis, which raises the mean error. Fig. 5(b) presents the error distribution for the four implemented quantizers. The boxplot shows the maximum, minimum and median error for each quantifier. All these errors are similar, regardless of the modulation used. Moreover, the error distribution is similar for all quantifiers and modulation indexes. There are some slight differences in the quartiles, but they are negligible. Consequently, we can state that the proposed fast quantizer does not significantly affect the H-ΣΔ modulation result.

B. Analysis of RCMV-ΣΔ

The efficiency of the proposed RCMV-ΣΔ techniques is analysed under different operating conditions. These modulations use the fast active quantizers proposed in Section III-A. Fig. 6 depicts the losses of the converter. Fig. 6(a) shows the transistor losses produced using the A-ΣΔ strategy. Transistor losses are less than 5.5 W for all operating points. Furthermore, the losses decrease as the modulation index increases. This behaviour is because high modulation indexes reduce the transitions between sectors and the switching. Fig. 6(b) illustrates the transistor losses generated by the RS-ΣΔ1&2 techniques. These modulations produce losses of less than 4.3 W for all operating points. As in the A-ΣΔ technique, losses decrease as the modulation index increases. However, this behaviour is less noticeable in the RS-ΣΔ1&2 strategies since their linear ranges are smaller. Fig. 6(c) shows the comparison between RS-ΣΔ1&2 and A-ΣΔ. The A-ΣΔ strategy generates more losses than RS-ΣΔ1&2 at low modulation indexes. However, the difference between the two modulations decreases significantly as the modulation index increases. This behaviour occurs because the RS-ΣΔ1&2 techniques only apply three vectors, while the A-ΣΔ strategy uses all the active vectors. Hence, RS-ΣΔ1&2 modulations only work with three regions, so they are less susceptible to variations in the reference and, thus, are more efficient than A-ΣΔ.

Fig. 7 details the switching behaviour of the proposed techniques. Fig. 7(a) shows the different switching frequencies during a grid period at $m = 0.5$. Moreover, this figure quantifies the number of commutations at each switching frequency. The A-ΣΔ technique principally works at 200, 133 and 100 kHz, while the RS-ΣΔ1&2 modulations switch at lower frequencies since they are less susceptible to variations in the reference. Fig. 7(b) illustrates the averaged switching frequency and the total switchings per transistor during a grid period. The bars plot the average switching frequency, while the lines represent the number of switchings. The number of commutations is higher in the A-ΣΔ technique for all operating points since this technique produces more losses than the RS-ΣΔ1&2 modulations. The number of commutations always decreases with the modulation index. Hence, the efficiencies increase with m. The average switching frequency follows a more unpredictable behaviour. In the A-ΣΔ technique, the frequency decreases with the modulation index, while in RS-ΣΔ1&2 modulations, the mean frequency increases with the index. From $m = 0.4$, the average frequency of RS-ΣΔ1&2 is higher than that of A-ΣΔ, but RS-ΣΔ1&2 techniques have less switchings and losses. Since the switching frequency is not uniform in ΣΔ techniques (see (23)), the average switching frequency is inadequate for studying the losses of these modulations.

The quality of the proposed modulations is analysed in terms of current harmonics. Fig. 8 compares the harmonics produced by the H-ΣΔ (with $r = 0.72$) and the proposed RCMV-ΣΔ techniques at 200 kHz and $m = 0.5$. The measurement considers only the first 40 harmonics, as detailed in the standard IEC 61000-3-2 [44]. Moreover, harmonics have been measured following the procedure indicated in IEC 61000-3-2 and IEC 61000-4-7 [45]. The plot does include homopolar currents, although they cannot flow through the load in three-phase three-wire power converters [46], [47]. All modulations produce harmonics below the maximums allowed by the standard. However, the proposed RCMV-ΣΔ techniques generate harmonics somewhat higher than the H-ΣΔ modulation, but the difference is not significant. Therefore, according to the results, the proposed RCMV-ΣΔ strategies do not increase either odd or even harmonic currents. Moreover, these techniques comply with the applicable harmonised standards.

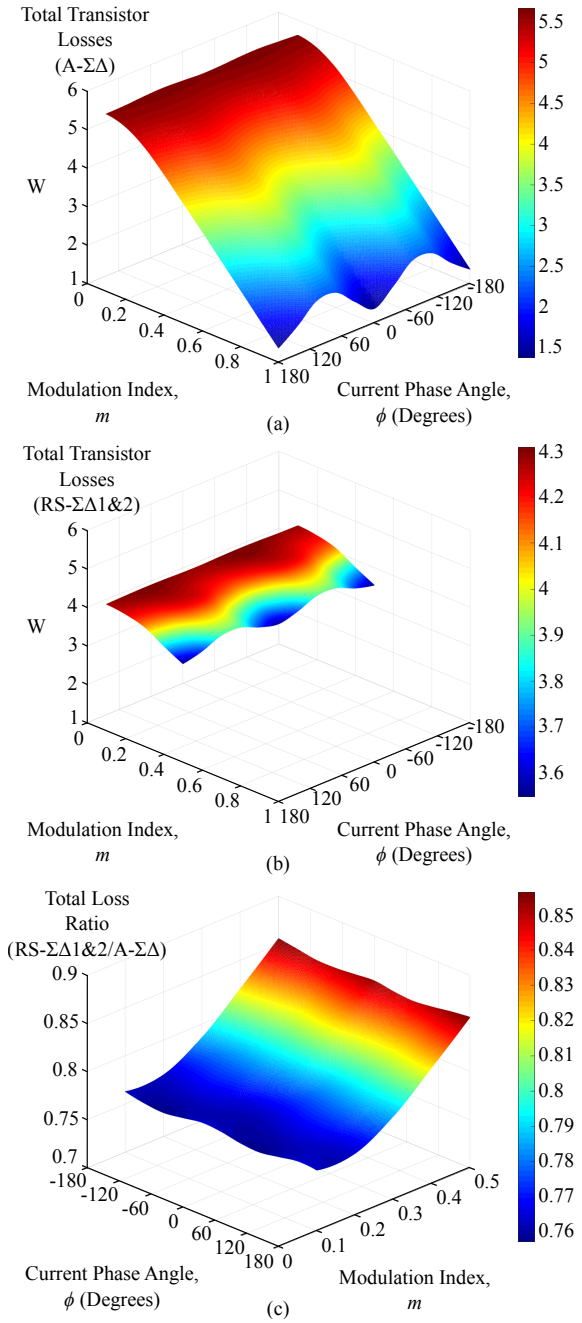

Fig. 6. Total losses at f_{max} = 200 kHz. (a) Losses of A-ΣΔ. (b) Losses of RS-ΣΔ1&2. (c) Ratio between RS-ΣΔ1&2 and A-ΣΔ.

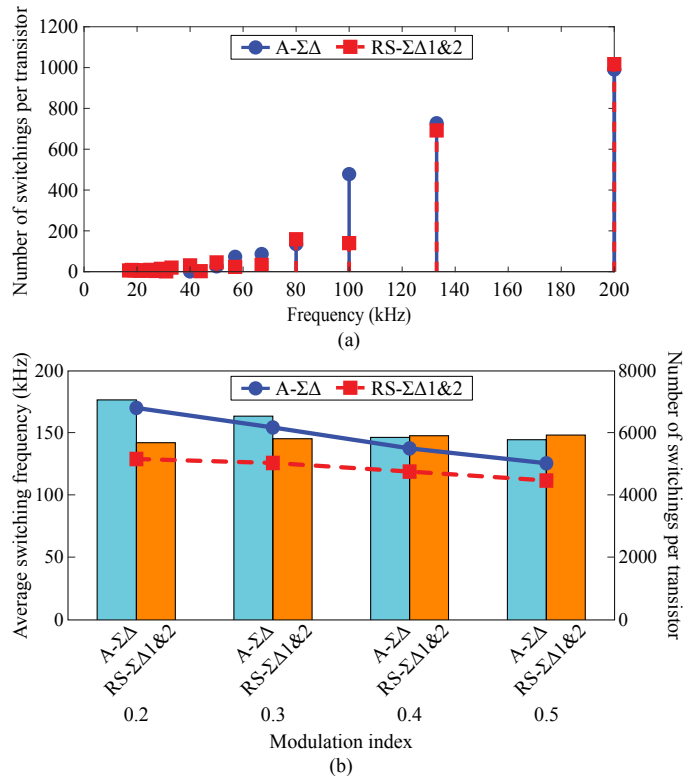

Fig. 7. Detail of the commutations of the A-ΣΔ and RS-ΣΔ1&2 strategies. (a) Swtiching frequencies at m = 0.5. (b) Average switching frequency and number of swtichings per transistor.

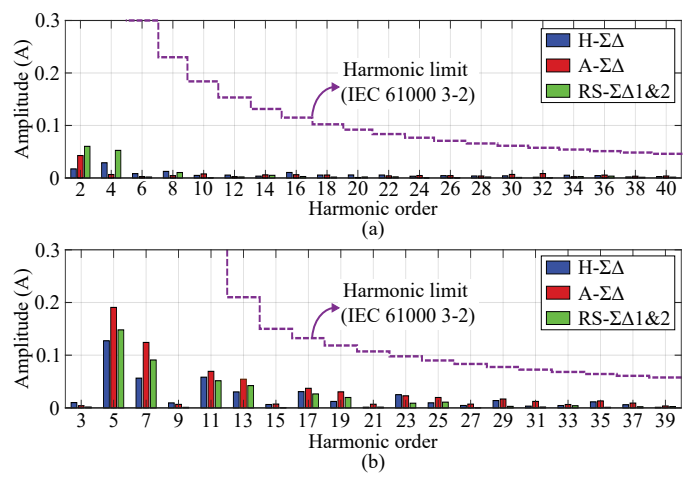

Fig. 8. Comparison of simulated current harmonics at f_{max} = 200 kHz. (a) Even harmonics. (b) Odd harmonics.

V. Experimental Results

To experimentally evaluate the proposed modulation techniques, we used a prototype that incorporated the previously simulated GaN e-HEMTs (GS66508T). This prototype has been designed to work with power ratings of up to 5 kW. A detailed explanation of the design of the converter, including an analysis of the parasitic inductances, can be found in [43]. On the ac side, there was a three-phase series-connected RL load with R = 45.3 Ω and L = 470 μH. On the dc side, there was a single-phase LISN (Electro-Metrics EM-7820) supplied by a constant 300-Vdc source. Another LISN (Rohde & Schwarz ESH3-Z5), connected to a 12-Vdc source, supplies the GaN converter. The modulation techniques were implemented on a dSPACE DS1006 platform and a DS5203 FPGA board. All the modulations use the fast active quantizers proposed in Section III-A. In the quantizer of the H-ΣΔ modulation, the radius is 0.72. Voltages were measured with a high-resolution oscilloscope (Agilent InfiniiVision MSO7104A: 1-GHz bandwidth and 4-GS/s sample rate), and high voltage differential probes (PMK BumbleBee: 400-MHz bandwidth). The common-mode current was measured using a current probe (HF-Stromwandler ESH 2-Z1). An EMI receiver (R&S

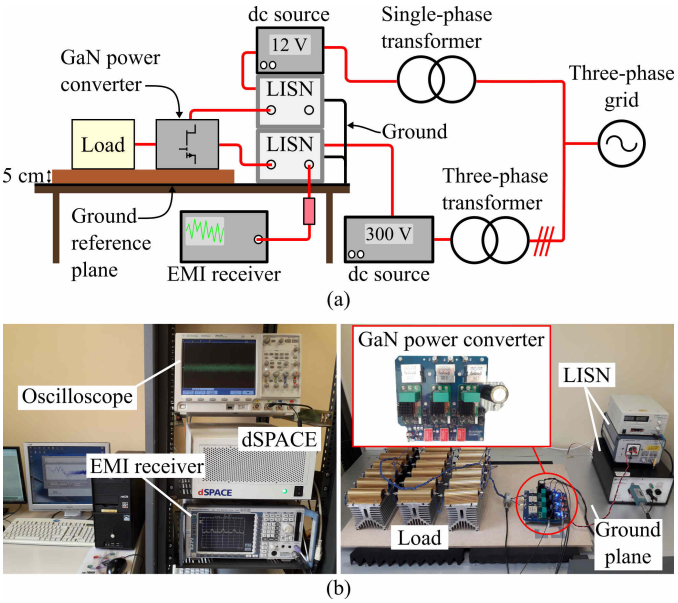

Fig. 9. View of the experimental setup. (a) Setup schematic. (b) Picture of the implemented setup.

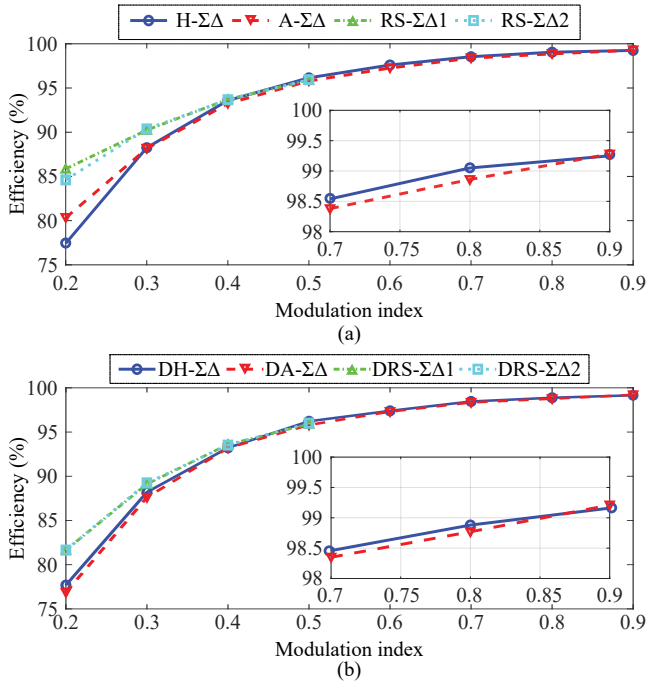

Fig. 10. Experimental converter efficiency curves at 200 kHz. (a) Efficiency of single-loop modulations. (b) Efficiency of double-loop techniques.

ESPI 9 kHz to 3 GHz) was used to obtain all the spectra. The converter efficiency was measured using a digital power meter (Yokogawa WT1600: 1-MHz bandwidth). Fig. 9 displays the experimental setup.

A. Experimental Performance

To evaluate the power loss reduction in RCMV-ΣΔ, we measured the efficiency of the different techniques. Fig. 10 illustrates the converter efficiency when using the proposed techniques at 200 kHz. Fig. 10(a) plots the efficiency of the single-loop modulations. At low modulation indexes, RS-ΣΔ1&2 techniques exhibit the best efficiency. At these operating points, H-ΣΔ and A-ΣΔ present similar losses. The efficiencies increase with the modulation index. All ΣΔ techniques show similar performances for modulation indexes greater than 0.4. H-ΣΔ and A-ΣΔ strategies have a maximum performance higher than 99%. Fig. 10(b) shows the efficiency of the modulations using two integrators. The acronym of these double-loop techniques is the same as the single-loop technique with a D. For example, the acronym of the double-loop A-ΣΔ strategy is DA-ΣΔ. These modulations behave similarly to their single-loop counterparts. However, the double-loop techniques exhibit slightly lower performances. Again, at low modulation indexes, the DRS-ΣΔ1&2 modulations offer the best efficiency, but from $m = 0.4$ upward, there are no significant differences between efficiencies. The maximum efficiencies of DH-ΣΔ and DA-ΣΔ are greater than 99%.

B. Experimental Harmonic Distortion

In order to analyse the quality of the proposed modulations at low frequencies, we compared the line-voltage THD produced by the RCMV-ΣΔ techniques with that obtained from the H-ΣΔ strategy. The THD measurement considers only the first 40 harmonics, as detailed in the standard EN 50160 [48].

Fig. 11 shows the line-voltage THD for different operating points. Fig. 11(a) shows the results obtained for the single-loop ΣΔ techniques. All of the studied techniques produce similar THDs for all operating points. The distortion of all modulations decreases with the modulation index. The H-ΣΔ technique exhibits the highest THD at low modulation indexes. However, the THD produced by H-ΣΔ is similar to that of A-ΣΔ at high modulation indexes. Fig. 11(b) presents the THDs of the double-loop ΣΔ strategies. The double-loop reduces harmonic distortion, and, therefore, these techniques exhibit lower THDs than their single-loop counterparts. There are no significant differences between the THDs of the analysed modulations. As in single-loop techniques, the THD of all double-loop strategies decreases with the modulation index.

Table VI presents in detail the experimental results shown by Figs. 10 and 11.

C. Experimental Electromagnetic Interference

To analyse the effect of the proposed RCMV-ΣΔ techniques, we compare the common-mode voltage, the common-mode current (CMC), and the conducted electromagnetic interference produced by these techniques with those obtained from the H-ΣΔ modulation. All of the results were obtained at $m = 0.5$. At this operation point, there are no notable differences between the EMIs produced by single-loop and double-loop strategies. Therefore, this article only includes the results of the double-loop techniques.

Fig. 12 shows the common-mode voltage waveform synthesized using the different ΣΔ strategies. DH-ΣΔ modulation shows the highest CMV among the studied techniques. The DH-ΣΔ strategy uses both zero vectors, so it does not limit the peak-to-peak CMV value nor the maximum CMV step height. In addition, this technique has an extremely high maximum

TABLE VI
DETAIL OF THE EXPERIMENTAL EFFICIENCY AND THD

Modulation technique		Efficiency (%)								THD (%)		
		Modulation index								Modulation index		
		0.2	0.3	0.4	0.5	0.6	0.7	0.8	0.9	0.2	0.5	0.8
Single-loop strategies	H-ΣΔ [36]	77.43	88.25	93.59	96.15	97.60	98.54	99.05	99.25	2.06	1.12	0.67
	A-ΣΔ	80.32	88.15	93.24	95.79	97.26	98.38	98.86	99.28	1.87	1.14	0.63
	RS-ΣΔ1	85.86	90.24	93.71	95.90	—	—	—	—	1.78	1.26	—
	RS-ΣΔ2	84.61	90.37	93.67	95.94	—	—	—	—	1.94	1.26	—
Double-loop strategies	DH-ΣΔ [36]	77.69	88.20	93.22	96.22	97.40	98.46	98.88	99.16	1.47	1.05	0.65
	DA-ΣΔ	76.87	87.61	93.20	95.80	97.31	98.35	98.77	99.21	1.44	1.04	0.63
	DRS-ΣΔ1	81.66	89.12	93.60	95.90	—	—	—	—	1.36	1.03	—
	DRS-ΣΔ2	81.65	89.25	93.52	96.01	—	—	—	—	1.48	1.03	—

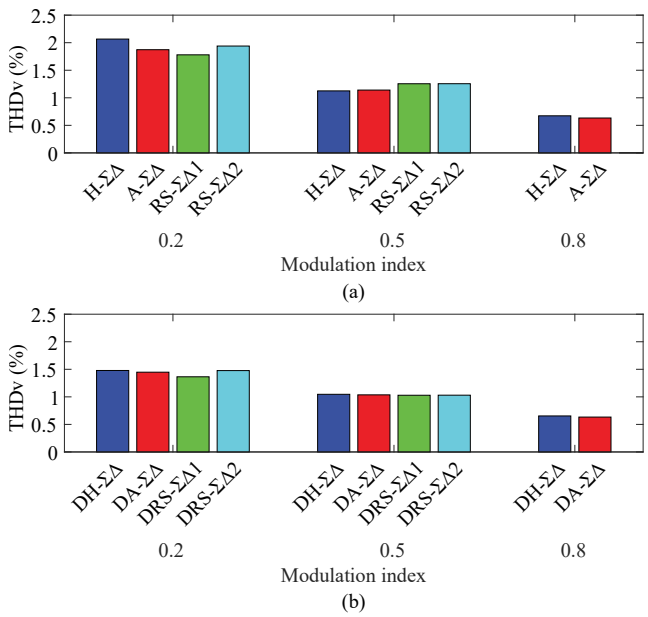

Fig. 11. Experimental THD of line voltage (V_{ab}) at 200 kHz. (a) THD of single-loop techniques. (b) THD of double-loop modulations.

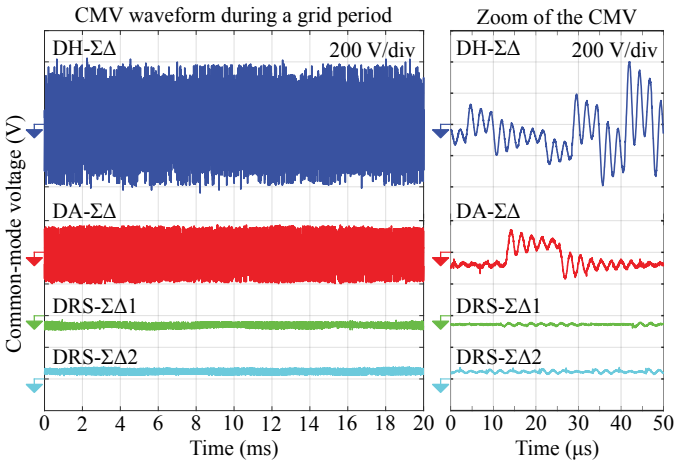

Fig. 12. Experimental CMV waveform synthesized using double-loop modulations.

CMV step height. These high steps produce the ringing observed in the CMV waveform. The DA-ΣΔ modulation generates lower voltages than DH-ΣΔ due to the absence of zero vectors. Hence, the CMV waveform of this technique only shifts between $+V_{dc}/6$ and $-V_{dc}/6$, so the ringing is low. Finally, both DRS-ΣΔ1&2 modulations generate a constant CMV equal to $\pm V_{dc}/6$. The CMV does not change since DRS-ΣΔ1&2 techniques only employ vectors that synthesize the same level of CMV.

Fig. 13 shows common-mode current and conducted EMI spectra produced by the proposed techniques. These measurements were performed according to the standard CISPR-16-1-1 [49]. From 9 to 150 kHz (Band A), the EMI receiver bandwidth was 200 Hz. From 0.15 to 30 MHz (Band B), the bandwidth was 9 kHz. As expected, DRS-ΣΔ1 and DRS-ΣΔ2 produce the same EMIs, so all the DRS-ΣΔ1&2 spectra shown are valid for both modulations.

Fig. 13(a) displays the CMC at band A. At 9 kHz, the studied modulations produce comparable CMC. However, the behaviour differs as the frequency increases. The CMC produced by the DRS-ΣΔ1 and DRS-ΣΔ2 techniques remains low for all frequencies. In contrast, the CMC level produced by the DH-ΣΔ and DA-ΣΔ techniques increases with frequency. The DA-ΣΔ modulation exhibits less CMC than DH-ΣΔ. However, from 80 kHz upwards, the CMC of these two techniques is very similar.

Fig. 13(b) plots the CMC at band B. The effect of the switching is seen in this figure since the maximum switching frequency is 200 kHz. All ΣΔ techniques spread the switching harmonics, so there are no significant spikes in the CMC. Overall, the DRS-ΣΔ1 and DRS-ΣΔ2 modulations produce the lowest CMC level among all the studied techniques. The DA-ΣΔ strategy also generates a lower level of CMC than DH-ΣΔ. Above 1 MHz, the difference between the proposed techniques becomes smaller. At high frequency, from 5 MHz upward, there are no significant differences among the modulation strategies.

Finally, Fig. 13(c) illustrates the conducted EMI generated by the proposed modulations. These techniques do not exhibit significant peaks in conducted EMI since the switching frequency is variable. Among the proposed modulations, the DRS-ΣΔ1&2 strategies generate the lowest electromagnetic distortion. This low noise is because CMC has a significant impact on total EMIs. For frequencies below 700 kHz, both DRS-ΣΔ1&2 strategies produce a noise level about 20 dB

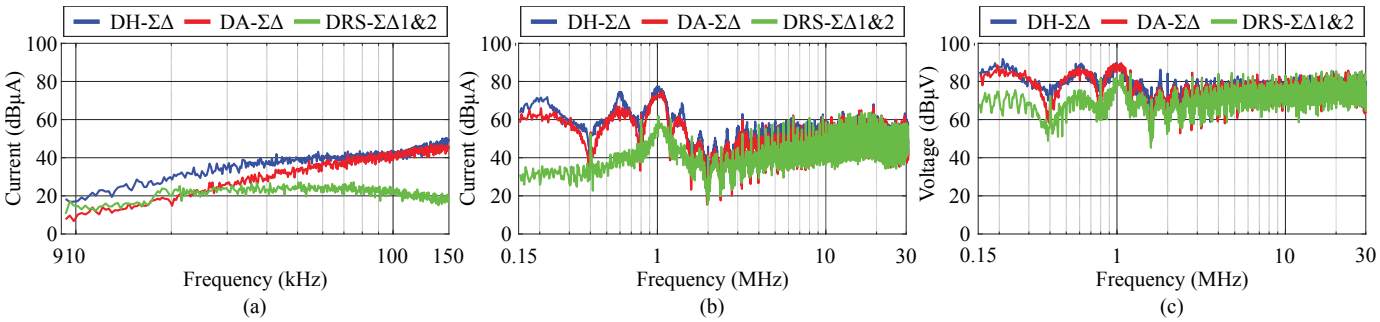

Fig. 13. Experimental spectra obtained at 200 kHz. (a) Common-mode current (Band A). (b) Common-mode current (Band B). (c) Conducted EMI.

TABLE VII
DETAIL OF THE EXPERIMENTAL EMI

Modulation technique	Maximum harmonic amplitude		
	Band A (dBμA)	Band B (dBμA)	Conducted EMI (dBμV)
DH-ΣΔ [36]	50.40	76.22	91.82
DA-ΣΔ	46.90	74.72	89.68
DRS-ΣΔ1&2	27.24	63.06	85.67

lower than the other techniques. DA-ΣΔ and DH-ΣΔ generate the same spectrum, but DA-ΣΔ is slightly better at some frequencies. Above 5 MHz, all of the studied modulations present similar noise level emissions.

Table VII presents the maximum harmonic amplitudes depicted by Fig. 13.

VI. Conclusion

This article proposes three RCMV-ΣΔ techniques for VSCs that use WBG power devices. These techniques are A-ΣΔ modulation, the RS-ΣΔ1 technique, and the RS-ΣΔ2 strategy. Moreover, this article proposes and validates the use of fast-processing quantizers for the RCMV-ΣΔ techniques and the classic H-ΣΔ modulations. These quantizers considerably simplify the implementation of ΣΔ modulations and reduce their computational cost. The effectiveness of the proposed techniques is demonstrated by the experimental results. RCMV-ΣΔ modulations are compared to the H-ΣΔ technique at different operating points using single and double loops. The results show that all RCMV-ΣΔ techniques improve the common-mode current at all frequency bands. Moreover, the proposed techniques reduce the conduced EMIs. Among the studied techniques, both RS-ΣΔ1&2 strategies exhibit the lowest EMI. These last modulations have a reduced linear range but, like similar PWM-based strategies, they can be useful in several applications such as electric motors [14], [50] and photovoltaic inverters [51]. On the other hand, A-ΣΔ offers a more modest EMI improvement without decreasing the linear range. The experiments demonstrate that RCMV-ΣΔ techniques have no significant disadvantages compared to H-ΣΔ modulation: they produce similar THDs and efficiencies. Therefore, the proposed modulations exhibit greater efficiencies than those of other spread-spectrum techniques without worsening the THD. Finally, this article concludes that the RCMV-ΣΔ modulations offer higher benefits than those of the H-ΣΔ strategy.

Acknowledgment

This work was supported by the Industrial Doctorates Plan of the Secretaria d'Universitats i Recerca del Departament d'Empresa i Coneixement de la Generalitat de Catalunya, the Centro para el Desarrollo Tecnológico Industrial (IDI-20200864), and the Ministerio de Ciencia, Innovación y Universidades of Spain within the project PID2019-111420RB-I00.

References

[1] J. Millan, P. Godignon, X. Perpina, A. Perez-Tomas, and J. Rebollo, "A survey of wide bandgap power semiconductor devices," *IEEE Transactions on Power Electronics*, vol. 29, no. 5, pp. 2155–2163, May 2014.

[2] K. Shenai, "High-Density Power Conversion and Wide-Bandgap Semiconductor Power Electronics Switching Devices," *Proceedings of the IEEE*, vol. 107, no. 12, pp. 2308–2326, Nov. 2019.

[3] K. Shenai, "Wide bandgap (WBG) semiconductor power converters for DC microgrid applications," in *2015 IEEE First International Conference on DC Microgrids (ICDCM)*. Atlanta, GA, USA: IEEE, Jun. 2015, pp. 263–268.

[4] F. Xue, R. Yu, and A. Q. Huang, "A 98.3% Efficient GaN Isolated Bidirectional DC-DC Converter for DC Microgrid Energy Storage System Applications," *IEEE Transactions on Industrial Electronics*, vol. 64, no. 11, pp. 9094–9103, Nov. 2017.

[5] T. Mishima and E. Morita, "High-Frequency Bridgeless Rectifier Based ZVS Multiresonant Converter for Inductive Power Transfer Featuring High-Voltage GaN-HFET," *IEEE Transactions on Industrial Electronics*, vol. 64, no. 11, pp. 9155–9164, Nov. 2017.

[6] J. Lu, K. Bai, A. R. Taylor, G. Liu, A. Brown, P. M. Johnson, and M. McAmmond, "A Modular-Designed Three-Phase High-Efficiency High-Power-Density EV Battery Charger Using Dual/Triple-Phase-Shift Control," *IEEE Transactions on Power Electronics*, vol. 33, no. 9, pp. 8091–8100, Sep. 2018.

[7] B. Li, Q. Li, F. C. Lee, Z. Liu, and Y. Yang, "A High-Efficiency High-Density Wide-Bandgap Device-Based Bidirectional On-Board Charger," *IEEE Journal of Emerging and Selected Topics in Power Electronics*, vol. 6, no. 3, pp. 1627–1636, Sep. 2018.

[8] A. K. Morya, M. C. Gardner, B. Anvari, L. Liu, A. G. Yepes, J. Doval-Gandoy, and H. A. Toliyat, "Wide bandgap devices in AC electric drives: Opportunities and challenges," *IEEE Transactions on Transportation Electrification*, vol. 5, no. 1, pp. 3–20, Mar. 2019.

[9] Z. Kaczmarczyk, M. Kasprzak, A. Ruszczyk, K. Sowa, P. Zimoch, K. Przybyła, and K. Kierepka, "Inductive Power Transfer Subsystem for Integrated Motor Drive," *Energies*, vol. 14, no. 5, p. 1412, Mar. 2021.

[10] A. Matallana, E. Ibarra, I. López, J. Andreu, J. I. Garate, X. Jordà, and J. Rebollo, "Power module electronics in HEV/EV applications: New trends in wide-bandgap semiconductor technologies and design aspects," *Renewable and Sustainable Energy Reviews*, vol. 113, p. 109264, Oct. 2019.

[11] Z. Waradzyn, R. Stala, A. Mondzik, A. Skała, and A. Penczek, "GaN-Based DC-DC Resonant Boost Converter with Very High Efficiency and Voltage Gain Control," *Energies*, vol. 13, no. 23, p. 6403, Dec. 2020.

[12] D. Han, S. Li, Y. Wu, W. Choi, and B. Sarlioglu, "Comparative Analysis on Conducted CM EMI Emission of Motor Drives: WBG Versus Si Devices," *IEEE Transactions on Industrial Electronics*, vol. 64, no. 10, pp. 8353–8363, Oct. 2017.

[13] B. Sun, R. Burgos, and D. Boroyevich, "Common-Mode EMI Unterminated Behavioral Model of Wide-Bandgap-Based Power Converters Operating at High Switching Frequency," *IEEE Journal of Emerging and Selected Topics in Power Electronics*, vol. 7, no. 4, pp. 2561–2570, 2019.

[14] E. Robles, M. Fernandez, J. Andreu, E. Ibarra, and U. Ugalde, "Advanced power inverter topologies and modulation techniques for common-mode voltage elimination in electric motor drive systems," *Renewable and Sustainable Energy Reviews*, vol. 140, no. January, p. 110746, Apr. 2021.

[15] T. Plazenet, T. Boileau, C. Caironi, and B. Nahid-Mobarakeh, "A Comprehensive Study on Shaft Voltages and Bearing Currents in Rotating Machines," *IEEE Transactions on Industry Applications*, vol. 54, no. 4, pp. 3749–3759, Jul. 2018.

[16] Y. Han, H. Lu, Y. Li, and J. Chai, "Analysis and Suppression of Shaft Voltage in SiC-Based Inverter for Electric Vehicle Applications," *IEEE Transactions on Power Electronics*, vol. 34, no. 7, pp. 6276–6285, Jul. 2019.

[17] M. S. Hassan, A. Abdelhakim, M. Shoyama, J. Imaoka, and G. M. Dousoky, "Three-Phase Split-Source Inverter-Fed PV Systems: Analysis and Mitigation of Common-Mode Voltage," *IEEE Transactions on Power Electronics*, vol. 35, no. 9, pp. 9824–9838, Sep. 2020.

[18] M. S. Hassan, A. Abdelhakim, M. Shoyama, J. Imaoka, and G. M. Dousoky, "Parallel Operation of Split-Source Inverters for PV Systems: Analysis and Modulation for Circulating Current and EMI Noise Reduction," *IEEE Transactions on Power Electronics*, vol. 36, no. 8, pp. 9547–9564, Aug. 2021.

[19] Y. Huang, J. Walden, A. Foote, H. Bai, D. Lu, F. Jin, and B. Cheng, "Analytical Characterization of CM and DM Performance of Three-Phase Voltage-Source Inverters Under Various PWM Patterns," *IEEE Transactions on Power Electronics*, vol. 36, no. 4, pp. 4091–4104, Apr. 2021.

[20] A. Hava and E. Un, "Performance Analysis of Reduced Common-Mode Voltage PWM Methods and Comparison With Standard PWM Methods for Three-Phase Voltage-Source Inverters," *IEEE Transactions on Power Electronics*, vol. 24, no. 1, pp. 241–252, Jan. 2009.

[21] C.-C. Hou, C.-C. Shih, P.-T. Cheng, and A. M. Hava, "Common-Mode Voltage Reduction Pulsewidth Modulation Techniques for Three-Phase Grid-Connected Converters," *IEEE Transactions on Power Electronics*, vol. 28, no. 4, pp. 1971–1979, Apr. 2013.

[22] K. Jayaraman and M. Kumar, "Design of Passive Common-Mode Attenuation Methods for Inverter-Fed Induction Motor Drive With Reduced Common-Mode Voltage PWM Technique," *IEEE Transactions on Power Electronics*, vol. 35, no. 3, pp. 2861–2870, Mar. 2020.

[23] J. Xu, J. Han, Y. Wang, M. Ali, and H. Tang, "High-Frequency SiC Three-Phase VSIs With Common-Mode Voltage Reduction and Improved Performance Using Novel Tri-State PWM Method," *IEEE Transactions on Power Electronics*, vol. 34, no. 2, pp. 1809–1822, Feb. 2019.

[24] R. Gamoudi, D. E. Chariag, and L. Sbita, "A Review of Spread-Spectrum-Based PWM Techniques - A Novel Fast Digital Implementation," *IEEE Transactions on Power Electronics*, vol. 33, no. 12, pp. 10 292–10 307, Dec. 2018.

[25] P. Lezynski, "Random Modulation in Inverters with Respect to Electromagnetic Compatibility and Power Quality," *IEEE Journal of Emerging and Selected Topics in Power Electronics*, vol. 6, no. 2, pp. 782–790, Jun. 2018.

[26] N. Chen, S. Yu, L. Gao, Y. Huang, and R. Chen, "Suppressing Interference Peak in an Active Power Filter via Periodic Carrier Frequency Modulation Based on a Spectrum Analysis Approach," *IEEE Transactions on Electromagnetic Compatibility*, vol. 61, no. 6, pp. 1760–1770, 2019.

[27] J. Chen, D. Jiang, W. Sun, Z. Shen, and Y. Zhang, "A Family of Spread-Spectrum Modulation Schemes Based on Distribution Characteristics to Reduce Conducted EMI for Power Electronics Converters," *IEEE Transactions on Industry Applications*, vol. 56, no. 5, pp. 5142–5157, Sep. 2020.

[28] S. Pavan, R. Schreier, and G. C. Temes, *Understanding Delta-Sigma Data Converters*, 2nd ed. Wiley-IEEE Press, 2017.

[29] E. Janssen and A. van Roermund, *Look-Ahead Based Sigma-Delta Modulation*, 1st ed. Dordrecht, Netherlands: Springer, 2011.

[30] J. Reiss, "Understanding Sigma-Delta Modulation: The Solved and Unsolved Issues," *AES: Journal of the Audio Engineering Society*, vol. 56, no. 1/2, pp. 49–64, Jan. 2008.

[31] G. Luckjiff, I. Dobson, and D. Divan, "Interpolative Sigma Delta Modulators for High Frequency Power Electronic Applications," in *Proceedings of PESC '95 - Power Electronics Specialist Conference*, Atlanta, GA, USA, 1995, pp. 444–449.

[32] I. H. Kheraluwala and D. M. Divan, "Delta Modulation Strategies for Resonant Link Inverters," *IEEE Transactions on Power Electronics*, vol. 5, no. 2, pp. 220–228, Apr. 1990.

[33] A. Mertens, "Performance Analysis of Three-phase Delta-Modulation Systems," *IEEE Transactions on Industry Applications*, vol. 30, no. 4, pp. 1016–1027, Aug. 1994.

[34] D. M. Divan, I. Dobson, and G. A. Luckiff, "Modulator for resonant link converters," pp. 2–4, 1997.

[35] G. Luckjiff and I. Dobson, "Hexagonal $\Sigma\Delta$ Modulators in Power Electronics," *IEEE Transactions on Power Electronics*, vol. 20, no. 5, pp. 1075–1083, Sep. 2005.

[36] D. Lumbreras, J. Zaragoza, N. Berbel, J. Mon, E. Galvez, and A. Collado, "Comprehensive Analysis of Hexagonal Sigma-Delta Modulations for Three-Phase High-Frequency VSC Based on Wide-Bandgap Semiconductors," *IEEE Transactions on Power Electronics*, vol. 36, no. 6, pp. 7212–7222, Jun. 2021.

[37] F. Acosta-Cambranis, J. Zaragoza, L. Romeral Martinez, and N. Berbel, "New Modulation Strategy for Five-Phase High-Frequency VSI based on Sigma-Delta Modulators." *IEEE Transactions on Power Electronics*, to be published. DOI: 10.1109/TPEL.2021.3121531.

[38] B. Jacob and M. R. Baiju, "A New Space Vector Modulation Scheme for Multilevel Inverters Which Directly Vector Quantize the Reference Space Vector," *IEEE Transactions on Industrial Electronics*, vol. 62, no. 1, pp. 88–95, Jan. 2015.

[39] T. N. Mir, B. Singh, and A. H. Bhat, "Delta-Sigma Modulation Based Common-Mode Voltage Elimination in Direct Matrix Converter," *IEEE Transactions on Industrial Informatics*, vol. 17, no. 2, pp. 1048–1057, 2021.

[40] J. Candy, "A Use of Double Integration in Sigma Delta Modulation," *IEEE Transactions on Communications*, vol. 33, no. 3, pp. 249–258, Mar. 1985.

[41] D. Holmes, "A general analytical method for determining the theoretical harmonic components of carrier based PWM strategies," in *Conference Record of 1998 IEEE Industry Applications Conference. Thirty-Third IAS Annual Meeting*, vol. 2, no. 2. St. Louis, MO, USA: IEEE, 1998, pp. 1207–1214.

[42] *PLECS User Manual*, 4th ed., Plexim GmbH, Zurich, Switzerland, 2019.

[43] D. Lumbreras, M. Vilella, J. Zaragoza, N. Berbel, J. Jordà, and A. Collado, "Effect of the Heat Dissipation System on Hard-Switching GaN-Based Power Converters for Energy Conversion," *Energies*, vol. 14, no. 19, p. 6287, Oct. 2021.

[44] *Electromagnetic compatibility (EMC) - Part 3-2: Limits - Limits for harmonic current emissions (equipment input current $\leq$16 A per phase). (IEC 61000-3-2:2018)*. EN 61000-3-2:2019, 2019.

[45] *Electromagnetic compatibility (EMC). Part 4-7: Testing and measurement techniques. General guide on harmonics and interharmonics measurements and instrumentation, for power supply systems and equipment connected thereto. (IEC 61000-4-7:2002)*. EN 61000-4-7:2002, 2002.

[46] P. Rodriguez, J. Pou, R. Pindado, J. Montanya, R. Burgos, and D. Boroyevich, "An Alternative Approach on Three-Dimensional Space-Vector Modulation of Three-Phase Inverters," in *2005 IEEE 36th Power Electronics Specialists Conference*, vol. 2005, no. 1. IEEE, 2005, pp. 822–828.

[47] D. Lumbreras, E. Gálvez, A. Collado, and J. Zaragoza, "Trends in Power Quality, Harmonic Mitigation and Standards for Light and Heavy Industries: A Review," *Energies*, vol. 13, no. 21, p. 5792, Nov. 2020.

[48] *Voltage characteristics of electricity supplied by public electricity networks*. EN 50160:2010, CENELEC, 2010.

[49] *Specification for radio disturbance and immunity measuring apparatus and methods - Part 1-1: Radio disturbance and immunity measuring apparatus - Measuring apparatus. (CISPR 16-1-1:2019)*. EN IEC 55016-1-1, CENELEC, 2019.

[50] J. Baik, S. Yun, D. Kim, C. Kwon, and J. Yoo, "Remote-State PWM with Minimum RMS Torque Ripple and Reduced Common-Mode Voltage for Three-Phase VSI-Fed BLAC Motor Drives," *Electronics*, vol. 9, no. 4, p. 586, Mar. 2020.

[51] T. K. S. Freddy, N. A. Rahim, W.-P. Hew, and H. S. Che, "Modulation Techniques to Reduce Leakage Current in Three-Phase Transformerless H7 Photovoltaic Inverter," *IEEE Transactions on Industrial Electronics*, vol. 62, no. 1, pp. 322–331, Jan. 2015.

David Lumbreras (Graduate Student Member, IEEE) received the B.S. degree in industrial technology engineering and the M.S. degree in automatic systems and industrial electronics engineering, in 2017 and 2018, respectively, from the Universitat Politècnica de Catalunya (UPC), Barcelona, Spain, where he is currently working toward the Ph.D. degree in electronic engineering with the Terrassa Industrial Electronics Group, Department of Electronic Engineering, UPC, Terrassa, Spain.

From July 2016 to January 2019, he was a CE Marking Engineer with the Certification Unit of Applus+ Laboratories Bellaterra, Spain. Since 2019, he has been a Researcher with the R&D Power Electronics, Circutor S.A., Viladecavalls, Spain. His research interests include modeling and control of power converters, multilevel converters, power quality, renewable energy, active power filters, electromagnetic compatibility, and modulation techniques.

Jordi Zaragoza (Member, IEEE) received the B.S. degree in electronic engineering, the M.S. degree in automatic and electronic industrial engineering, and the Ph.D. degree from the Universitat Politècnica de Catalunya (UPC), Catalonia, Spain, in 2001, 2004, and 2011 respectively.

In 2003, he joined as an Assistant Professor with the Faculty of UPC, where he became an Associate Professor in 2012. From 2006 to 2007, he was a Researcher with the Energy Unit of ROBOTIKER-TECNALIA Technologic Corporation, Basque Country, Spain. Since 2017, he has been the Director of the Terrassa Industrial Electronics Group, UPC. He is the author of more than 70 published technical papers and has been involved in several projects in the fields of power electronics and systems. His research interests include modeling and control of power converters, multilevel converters, wind energy, power quality, and HVdc transmission systems.

Néstor Berbel received the B.S., M.S., and Ph.D. degrees from the Universitat Politècnica de Catalunya (UPC), Barcelona, Spain, in 2002, 2004, and 2015, respectively, all in electronic engineering.

In 2003, he joined as an Assistant Professor with the Faculty of UPC, where he became an Associate Professor in 2012. His scientific research has been developed at the Terrassa Industrial Electronics Group, Department of Electronic Engineering, UPC, Terrassa, Spain. His research interests include microelectronic reliability, power converters, efficiency on power converters, modulations and control loops applied on power converters.

Juan Mon was born in Galicia, Spain, in 1977. He received the M.S., and Ph.D. degrees in electronics engineering from the Universitat Politècnica de Catalunya (UPC), Barcelona, Spain, in 2005 and 2012, respectively.

In 2000, he joined the faculty of UPC as an Assistant Professor with the Department of Electronics Engineering. His main research interest is the electromagnetic compatibility in power converters.

Eduardo Gálvez was born in Sevilla, Spain. He received the M.S. degree in telecomunications engineering from the Universitat Politècnica de València (UPV), Valencia, Spain in 2000.

From 2000 to 2002, he worked as Probe Test Engineer at Analog Devices, Limerick, Ireland. From 2003 to 2005, he worked as electronic products Supplier Quality Engineer at Ficosa, Barcelona, Spain. Since 2005, he has been with Circutor S.A., Viladecavalls, Spain, as a Development Engineer at Zurc Development Center. From 2010 to 2015 as Engineering Manager of Zurc, where he has been a Power Electronics Engineering Manager with the Circutor Development Center since 2014. He also holds two patents.

Alfonso Collado received the B.S. degree in electronics engineering from the Universitat Politècnica de Catalunya (UPC), Barcelona, Spain, in 1989.

From 1986 to 1989, he was a Research Technician with Instrumentacion Industrial Zurc, Viladecavalls, Spain, where he become a Technical Manager from 1989 to 2010. Since 2010, he is an R&D&i Manager with Circutor S.A., Viladecavalls, Spain. For the last three years, he has been working specially in innovative technologies and how to apply these to the new products developed by the company. His main research interests include energy efficiency, power conversion efficiency, renewable energy, electric vehicles, and the new IoT opportunities to improve the consumer's behavior about how to be more efficiency managing his consumptions.